



HAL
open science

Versatile, fast, and accurate frequency excursions with a semiconductor laser

Thomas Llauze, Félix Montjovet-Basset, Anne Louchet-Chauvet

► To cite this version:

Thomas Llauze, Félix Montjovet-Basset, Anne Louchet-Chauvet. Versatile, fast, and accurate frequency excursions with a semiconductor laser. *Applied optics*, 2024, 63 (19), pp.5192. 10.1364/AO.522789 . hal-04727631

HAL Id: hal-04727631

<https://hal.science/hal-04727631v1>

Submitted on 9 Oct 2024

HAL is a multi-disciplinary open access archive for the deposit and dissemination of scientific research documents, whether they are published or not. The documents may come from teaching and research institutions in France or abroad, or from public or private research centers.

L'archive ouverte pluridisciplinaire **HAL**, est destinée au dépôt et à la diffusion de documents scientifiques de niveau recherche, publiés ou non, émanant des établissements d'enseignement et de recherche français ou étrangers, des laboratoires publics ou privés.

Versatile, fast and accurate frequency excursions with a semiconductor laser

THOMAS LLAUZE,¹ FÉLIX MONTJOVET-BASSET,² AND ANNE LOUCHET-CHAUVET^{1,*}

¹ESPCI Paris, Université PSL, CNRS, Institut Langevin, 75005 Paris, France

²Chimie ParisTech, PSL University, CNRS, Institut de Recherche de Chimie Paris, Paris, 75005, France

*anne.louchet-chauvet@espci.fr

Abstract: Achieving accurate arbitrary frequency excursions with a laser can be quite a technical challenge, especially when steep slopes (GHz/ μ s) are required, due to both deterministic and stochastic frequency fluctuations. In this work we present a multi-stage correction combining four techniques: pre-distorsion of the laser modulation, iterative correction, opto-electronic feedback loop and feed-forward correction. This combination allows not only to compensate for the non-instantaneous response of the laser to an input modulation, but also to correct in real time the stochastic frequency fluctuations. We implement this multi-stage architecture on a commercial DBR laser and verify its efficiency, first with monochromatic operation and second with highly demanding frequency excursions. We demonstrate that our multi-stage correction not only enables a strong reduction of the laser linewidth, but also allows steep frequency excursions with a relative RMS frequency error well below 1%, and a laser spectral purity consistently better than 100 kHz even in the midst of GHz-scale frequency excursions.

1. Introduction

The ability to rapidly and precisely tune the frequency of a laser, known as "agility", is key for a large number of applications like FMCW lidar [1, 2], rapid wavelength switching in telecommunications [3], wideband optical signal processing [4] and quantum applications [5].

The simplest approach to generate fast laser frequency chirps is to directly modulate the wavelength of a laser. Extended cavity diode lasers (ECDL) are widely tunable, but this tunability relies on the mechanical movement of a grating or mirror, which limits both reproducibility and tuning speeds to a few hundred Hz or below. The addition of an intra-cavity electro-optical element has been proposed to overcome these limitations [6], but the modulation bandwidth is then constrained by its piezoelectric resonances [7]. Conversely, silicon nitride-based photonic integrated circuits enable impressive chirp rates in the THz/ μ s range [8] with up to 500 MHz modulation frequencies, but with major chirp non-linearity. Finally, monolithic semiconductor lasers (such as DBR or DFB architectures) allow for extended continuous tuning range via the external control of their injection current [9, 10], while the corresponding modulation bandwidth can be as high as 100 MHz [11] thanks to the very short carrier lifetime in such structures [12]. Nevertheless, the precision of the frequency excursions decreases with their steepness.

Fast frequency chirps can also be created from any monochromatic laser by single sideband external phase modulation [13], which offers ideal modulation linearity and control of the frequency and amplitude of the optical signal waveform. Serrodyne driving of an external phase modulator in the path of a monochromatic laser beam is also an efficient way to achieve precise frequency shifting [14], but its implementation at the GHz level imparts severe requirements on the arbitrary waveform generation [15]. In any case, for all external modulation techniques, jitter and frequency noise of the seed laser are likely to lead to stochastic frequency fluctuations that eventually impair the sweep linearity.

Therefore, it appears necessary to deploy versatile and effective tools to enhance the linearity and precision of fast laser frequency scans. Several complementary methods have already been proposed. The pre-distorsion of the command sent to the laser source, based on prior

measurement of the modulation input transfer function, corrects the deviations caused by the non-instantaneous response of the laser [16–18]. An iterative correction allows to compensate for the frequency deviations due to the nonlinear part of the laser’s response [17–20]. Finally, an improvement in the chirps precision is possible through real-time feedback correction [7, 16, 17, 21] that addresses the stochastic frequency noise associated either with the intrinsic laser or triggered by the frequency sweep. Interestingly, these three methods are not specific to a particular laser design. However, despite impressively high chirp linearity demonstrated using such correction methods [18, 20, 21], their operational range is limited to modulation frequencies below a few hundred kHz, typically. This limitation renders them compatible only with relatively slow chirps or rather gentle slope changes.

In this paper, we propose a multi-stage method to achieve precise chirps at the GHz/ μ s scale. The method encompasses (i) a pre-distorsion followed by (ii) an iterative optimization of the voltage command used to achieve the frequency excursions, a (iii) opto-electronic feedback loop and (iv) a feed-forward correction of the instantaneous laser frequency. While each of these stages has been used previously to linearize frequency chirps or reduce laser linewidth, as evidenced by prior works [20–26], our novel contribution lies in the comprehensive combination of these four techniques allowing a robust and versatile operation, capable of addressing both monochromatic operation and arbitrary frequency excursions with steep chirps.

In section 2, we briefly present the twofold correction method designed to compensate for the systematic deviations to the frequency excursion, including the pre-distorsion based on the laser transfer function, and the iterative correction stage. This method relies on a non-ambiguous measurement of the laser instantaneous frequency. Section 3 is devoted to the description of the real-time correction stage addressing the stochastic deviations to the intended frequency excursion. This correction includes a feedback loop and a feed-forward correction. We demonstrate the potential of this multi-stage architecture by implementing triangular chirps with various amplitudes and modulation frequencies, and an arbitrary frequency excursion involving alternating steep frequency variations and monochromatic operation. We show that a relative RMS frequency error better than 1% of the total excursion range can be achieved, including the abrupt slope changes. This demonstration utilizes a commercial DBR laser but could be transposed to any rapidly tunable laser.

2. Correcting systematic laser frequency deviations

2.1. Generating and measuring fast frequency excursion

Modulating the frequency of a semiconductor laser by varying the bias current in the laser’s gain section leads to strong imperfections, primarily stemming from the non-instantaneous nature of the laser reaction to changes in its bias current. These imperfections can manifest as unwanted non-linearities in the frequency chirps [27]. In order to quantify and correct such imperfections, an access to the laser’s instantaneous frequency variations is required. The quality of the frequency excursion will then be estimated by measuring the RMS frequency error with respect to the desired frequency excursion. An interesting figure of merit is the relative RMS, defined as the ratio between this RMS frequency error and the total excursion frequency range.

The instantaneous frequency can be obtained using an unbalanced Mach-Zehnder interferometer (MZI) with an optical delay τ_{MZI} and a frequency shift f_{MZI} in one of its arms (see Figure 1). We finally collect the beatnote signal on a photodiode at the output of the MZI. For an incoming laser field $E(t) = E_0 e^{i(2\pi\nu_0 t + \phi(t))}$, $\phi(t)$ being the instantaneous phase of the laser, the beatnote signal at the output of the MZI reads as:

$$V(t) \propto 1 + \sin(2\pi f_{\text{MZI}} t + \phi(t - \tau_{\text{MZI}}) - \phi(t)) \quad (1)$$

The instantaneous frequency $f(t)$, defined as $f(t) = \frac{1}{2\pi} \frac{d\phi(t)}{dt}$, may then be retrieved from $V(t)$ using the Hilbert transformation [28].

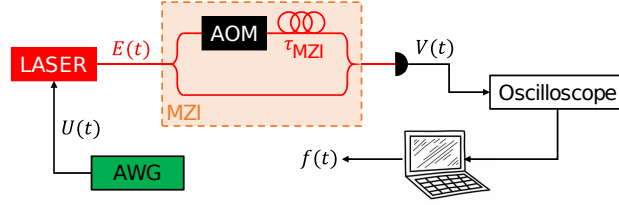


Fig. 1. Optical setup for instantaneous laser frequency measurement. An arbitrary waveform generator (AWG) issues the voltage command $U(t)$ sent to the laser source. The laser field $E(t)$ enters an unbalanced Mach-Zehnder interferometer (MZI) containing an acousto-optic modulator (AOM) inducing a frequency shift in its long arm. The beatnote $V(t)$ collected on the photodiode is digitized and processed to retrieve the instantaneous laser frequency $f(t)$.

2.2. Distorted laser response and corresponding correction

When the laser frequency is modulated via a modulation input on its current supply, a voltage command $U_0(t)$ leads to a distorted frequency excursion $f(t)$. Assuming the laser and current supply operate linearly, this frequency excursion is given by the convolution product of the voltage command and the impulse response $R(t)$ of the system:

$$f(t) = U_0(t) \otimes R(t) \quad (2)$$

To make the laser operate according to the user's requirement, one can fully characterize the laser and driver's impulse response $R(t)$ (or, equivalently, its transfer function $H(f)$ expressed in Hz/V), and consequently operate the laser with a pre-distorted voltage command $U_{pd}(t)$ given by:

$$U_{pd}(t) = \mathcal{F}^{-1} \left[\frac{\mathcal{F}[f_C(t)](f)}{H(f)} \right] \quad (3)$$

where $f_C(t)$ is the desired frequency excursion and \mathcal{F} is the Fourier transform operator.

In the linear regime, such a pre-distortion ideally compensates for reproducible laser frequency deviations originating from the non-instantaneous response of the laser and driver. However, residual errors may remain due to the effective non-linear response the laser frequency to the injection current [29]. To address this, an efficient method consists in iteratively modifying the voltage command with a small correction inferred from the previously measured frequency error [17, 18]. More specifically, the i -th voltage command is obtained as:

$$U_i(t) = \mathcal{F}^{-1} \left[\frac{[\mathcal{F}[U_{i-1}(t)](f)H(f) + \alpha \mathcal{F}[\epsilon_{i-1}(t)](f)]}{H(f)} \right], \quad (4)$$

$U_{i-1}(t)$ being the previous voltage command, $\epsilon_{i-1}(t)$ the previous frequency error with respect to the desired frequency excursion, and α a numerical parameter chosen between 0 and 1 to ensure the convergence.

2.3. Experimental realisation

We implement the aforementioned double correction scheme on a Photodigm PH795DBR laser operating at 793.4 nm. Voltage commands are sent to the fast modulation input of the laser current driver (Vescent D2-105), therefore directly addressing the gain section. The successive voltage commands are generated with an arbitrary waveform generator (Tektronix AWG5004). The power variation associated to such a modulation is below 1%. The fully fibered, unbalanced MZI comprises an optical delay $\tau_{\text{MZI}} = 60$ ns and a 80 MHz AOM in the same arm. The beatnote

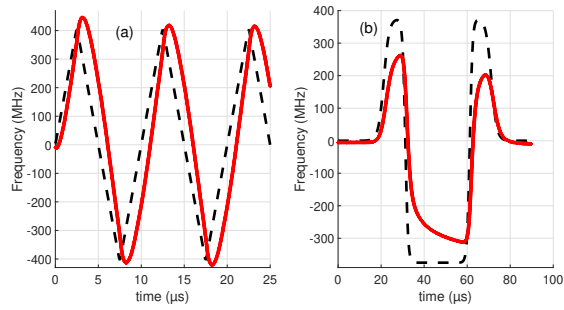


Fig. 2. Evidence of the non-instantaneous laser response (solid red line) to a rapidly varying drive voltage (black dashed line), in the case of (a) triangular and (b) arbitrary command.

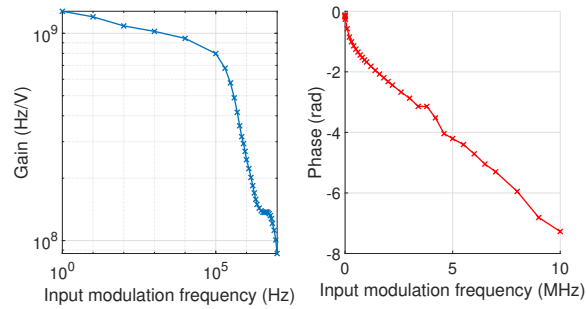


Fig. 3. Laser transfer function amplitude and phase when disturbed through the "Current Servo Input" modulation input of the Vescent D2-105 driver. The laser instantaneous frequency is measured with the unbalanced, frequency-shifting MZI. Therefore this transfer function includes the response of this modulation input, that of the laser itself, and the response of the MZI.

signal is collected on a 150 MHz bandwidth photodiode, sampled with a digital oscilloscope and transferred to a computer to derive the instantaneous frequency of the laser $f(t)$ [28].

Two types of excursion are tested: first, a periodic, triangular frequency excursion comprised of two opposite chirps, with a 800 MHz chirp span and 100 kHz modulation frequency. Second, an arbitrary excursion with two opposite $2.5 \mu\text{s}$ -long chirps over a 750 MHz range, corresponding to a $300 \text{ MHz}/\mu\text{s}$ chirp rate, separated by a $20 \mu\text{s}$ monochromatic operation interval (see Figure 2). The drive voltage and the corresponding laser response show a strong distortion, with frequency errors as high as 300 MHz. In the triangular case, we measure a 72.9 MHz RMS frequency error, *ie* a 9.1% relative RMS.

In order to implement the pre-distortion stage, we determine the laser transfer function $H(f)$ in amplitude and phase by sending sinusoidal voltages into the modulation input of the laser current controller and measuring the resulting instantaneous frequency variation of the laser (see Fig. 3). The voltage commands corresponding to triangular and arbitrary frequency excursions are then pre-distorted using Eq. 3. The pre-distortion, operating as an anticipation of the non-instantaneous laser response, leads to a significant improvement of the laser behaviour (see Figure 4): the frequency errors are clearly reduced (of the order of 60 MHz). For the triangular chirps, the RMS frequency error is reduced to 20.52 MHz, equivalent to a 2.5% relative RMS.

In order to further reduce the frequency error, we implement the iterative correction algorithm on both frequency excursions using Equation 4 (see Figure 4). We observe that after few tens

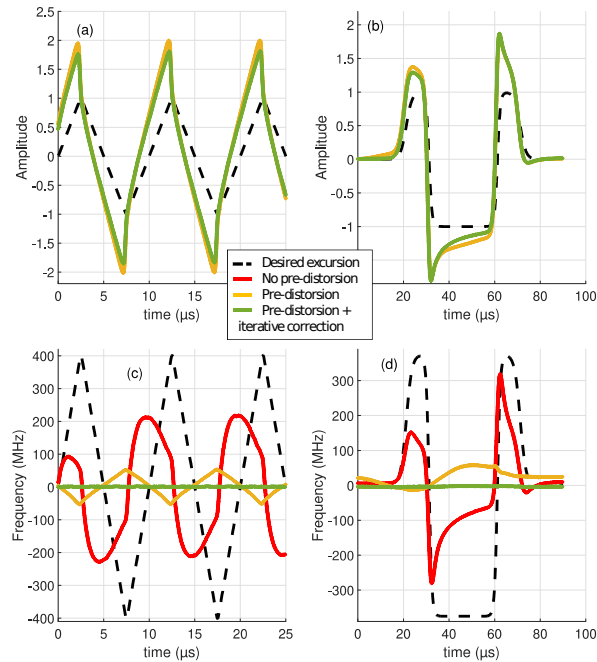


Fig. 4. Pre-distorted voltage commands (yellow line) and iteratively-corrected voltage commands (green line) in order to achieve the desired frequency excursions (black dashed line), in the case of (a) triangular and (b) arbitrary excursion. (c) and (d): frequency errors with a free-running laser (red line), with the pre-distorsion (yellow line) and after 20 iterations (green line).

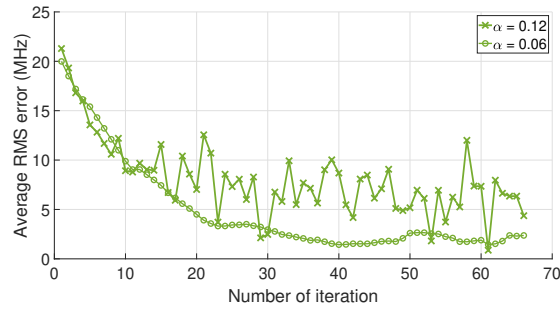


Fig. 5. Evolution of the RMS frequency error using the iteration algorithm described in Equation 4, in the case of a triangular 800 MHz amplitude frequency excursion with 100 kHz modulation frequency, for two values of the parameter α .

of iterations, the frequency error is substantially reduced, down to a few MHz. A 2.1 MHz RMS frequency error is obtained for the triangular chirps, corresponding to a 0.26% relative RMS. Examining the convergence of the iterative algorithm, we show that larger α values allow a faster convergence but a lower frequency excursion precision (see Figure 5).

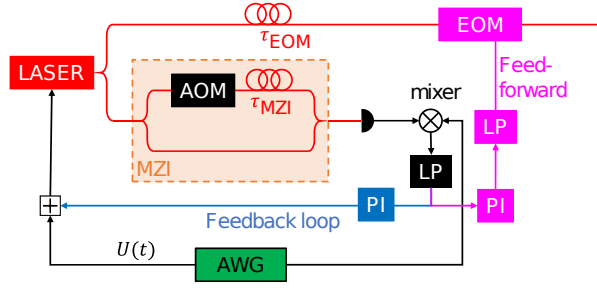


Fig. 6. Experimental setup including the feedback loop and the feed-forward correction for arbitrary frequency excursions. The laser current is driven via an arbitrary voltage command generated by an arbitrary waveform generator (AWG) fed into a fast modulation input port. For both corrections, an error signal is produced via the down-conversion of the beatnote at the output of the self-heterodyne MZI. For the feedback loop, this error signal is filtered through a proportional-integrator filter (PI) and added to the voltage command to the laser current driver. For the feed-forward correction, the same error signal is filtered with a PI and a low pass filter (LP), and fed into a electro-optic phase modulator (EOM) after a physical fibered delay line on the user laser beam.

3. Suppression of non-reproducible errors

Once the systematic errors are efficiently suppressed, one is left with only stochastic frequency errors, mostly coming from the intrinsic laser frequency noise, but also potentially caused by the steep frequency chirps and abrupt slope changes. We propose a versatile correction able to handle arbitrary frequency commands including fast laser chirps and monochromatic laser operation.

3.1. Phase-Locked-Loop feedback correction

Self-heterodyne systems (such as the unbalanced MZI presented in Section 2.1) enable the generation of a signal proportional to the frequency offset via the downconversion of the detected beatnote with a local oscillator (LO). This signal can then be used as a correction signal to the laser source, resulting in a feedback loop. This setup is analog to an electronic phase-locked-loop (PLL) where the voltage-controlled oscillator (VCO) is composed of the laser source and the interferometer, and the frequency mixer and subsequent filter act as a phase comparator.

We use a versatile version of this setup that consists in using a specific local oscillator $V_{th}(t)$, proportional to the ideal beatnote signal that is expected for an ideal, error-free and noise-free laser frequency excursion, given any arbitrary laser frequency excursion [16].

We experimentally implement this PLL feedback loop using the optical beatnote collected at the output of the MZI (see Section 2.1) and mixing it with the ideal beatnote signal generated by our multichannel AWG5004, using an electronic mixer (Mini-Circuits ZFM.1+). The use of a different channel from the same AWG for driving the AOM and creating the LO signal ensures minimal electronic jitter. The resulting signal is filtered with a 10-MHz, 5th order Tchebychev low-pass filter. A proportional-integrator loop filter is then used, built with a Newport LB1005S servo-controller operated in Low Frequency Gain Limitation (LFGL) mode with a 1-MHz PI corner.

The transfer function of the closed feedback loop is measured and plotted in Figure 7. A description of the measurement method is given in Appendix A. We observe a sharp cutoff around 600 kHz. The PLL transfer function exhibits a quasi-linear phase, whose slope corresponds to

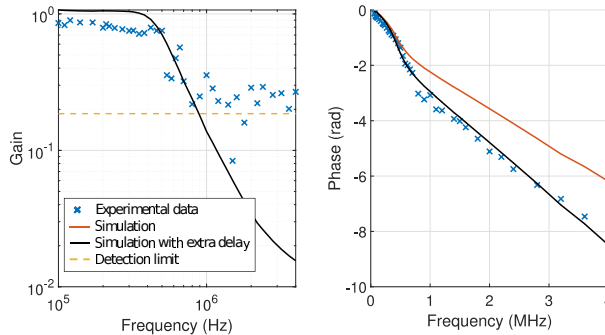


Fig. 7. Experimental (dots) and simulated (lines) closed feedback loop transfer function in amplitude (a) and phase (b). The simulated transfer function is derived from the independent measurement of each component of the loop (see Appendix A.1), completed with an additional delay (black lines). The red line shows the transfer function phase without this additional delay. The yellow dashed line shows the detection noise limit.

an effective group delay $\tau_{PLL} = 270$ ns where $\Phi(f) = 2\pi f \tau_{PLL}$. We demonstrate in Appendix A that this delay corresponds to the physical delay of the various optical and electronic elements in the loop, and that it directly affects the feedback bandwidth via $BW = \frac{1}{8\tau_{PLL}} \approx 460$ kHz.

3.2. Feed-forward correction

The high frequency fluctuations triggered by fast frequency excursions require an instantaneous frequency correction with a broad bandwidth. To overcome the feedback bandwidth limitation, we propose to combine it with a feed-forward (FF) correction. Feed-forward consists in applying a correction to the laser emission a posteriori, using the knowledge of the current laser behaviour. To achieve this, a phase-modulating device must be used, such as an electro-optic modulator (EOM) or acousto-optic modulator (AOM). An EOM offers a weaker tunability than an AOM but a higher bandwidth, which is key for the correction of high frequency errors. The FF approach has already been proposed for laser linewidth narrowing, either independently [30] or in combination with feedback [25, 26].

In our design, we propose to generate a FF correction based on the same error signal as the feedback loop after the downconversion step. This error signal is sent to the phase modulator inserted in the user beam (see Fig. 6), after appropriate electronic filtering. Importantly, the quality of the FF correction relies on the application of the correction at the right time. Therefore, to account for the delay naturally occurring in the buildup of the correction signal, a physical delay is inserted before the phase modulator along the user beam.

We implement the FF scheme using a fibered electro-optic fibered phase modulator (iXblue MPXLN-0.3) with 300 MHz bandwidth. The FF correction signal is obtained using the same error signal as the PLL fed into a specific feed-forward filter composed of another Newport LB1005S servo-controller operated in LFGL mode (1MHz PI-corner) and a low-pass RC filter with 10 MHz cutoff frequency. The combination of all the optical and electronic elements of the feed-forward correction yields a high-pass behaviour and a total group delay of around 180 ns (see Appendix B). In order for the FF correction to reach the laser emission at the right time, a 28 m fibered delay line (corresponding to a 140 ns delay) is inserted before the EOM.

We investigate the influence of this physical delay on the quality of the noise compensation and show that it has a critical effect on the quality of the feed-forward correction and in turn on the laser linewidth (see Appendix B). Interestingly, in contrast with the feedback correction,

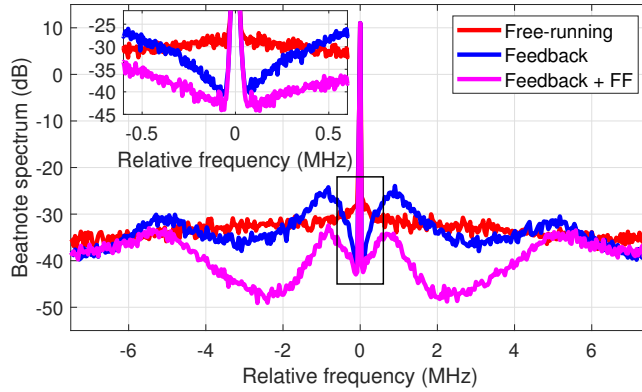


Fig. 8. Self-heterodyne beatnote spectra with a monochromatic laser (resolution bandwidth: 10 kHz) for various experimental configurations. The beatnote spectrum is centered on the 80 MHz driving frequency of the AOM inside the MZI (see Fig. 1). Inset: close-up view showing the feedback bandwidth.

the feed-forward bandwidth is only limited by the bandwidth of the various elements of the FF correction signal and remains independent from the feed-forward delay as long as the latter is perfectly matched by the physical delay.

3.3. Implementation on a monochromatic laser

Our dynamic, real-time corrections are tested on the DBR laser in monochromatic operation. In Figure 8 we plot the power spectral density (PSD) of the beatnote signal with and without feedback correction. We obtain a noise rejection of about 10 dB in a 150 kHz range around the carrier frequency. One can derive the feedback bandwidth as the frequency at which the beatnote signal PSD reaches the value of the free-running laser beatnote PSD. Such an estimation yields a feedback bandwidth around 400 kHz, in agreement with the bandwidth derived from the closed loop transfer function (see Section 3.1).

Assessing the influence of the FF correction on the laser spectral purity is less straightforward. Indeed, a second optical frequency discriminator (OFD) is needed [25]. However, using a separate, independent device would lead to relative instability due to uncorrelated acoustic and thermal perturbations. To avoid this we use the *same* physical OFD as the one used for the error signal generation (see Fig. 9): we simultaneously send the feed-forward-corrected laser beam in the unused port of the MZI, in the backwards direction. The effect of the full correction can then be analyzed via the spectrum of the beatnote collected on the second photodiode (see Figure 8). We demonstrate a 5 MHz correction bandwidth for the combined feedback and feed-forward stages. The maximum noise rejection (15dB) occurs at 2.4 MHz from the carrier frequency.

We can also analyze the performance of our feedback and feed-forward corrections by examining the laser linewidth and laser spectrum that we derive from the output of a commercial optical frequency discriminator (Silentsys OFD) [31] (see Figure 10). We observe the typical linewidth tendency to increase with the integration time [32], in all configurations. The feedback has a crucial impact on the linewidth on the investigated timescales (above 10 μ s). The feed-forward correction, on the other hand, is most efficient on shorter timescales where the linewidth cannot be accurately measured. The 740-kHz linewidth of the free-running laser for a 100 ms integration time is reduced down to 81 kHz with the feedback correction, and further down to 30 kHz with both the feedback and the feed-forward corrections. This value is only marginally larger than the laser's 10 kHz Lorentzian linewidth limit attributed to the white part of its residual frequency noise [33].

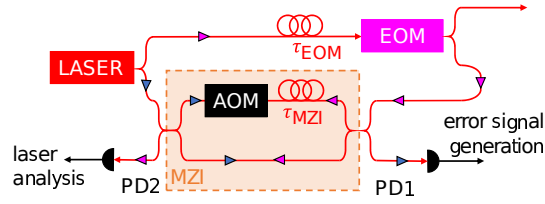


Fig. 9. Simultaneous error signal generation and instantaneous laser frequency measurement with a single MZI: the MZI is assembled with 2×2 3dB fiber couplers allowing two opposite, independent propagation schemes in the same equipment and ensuring perfect relative stability.

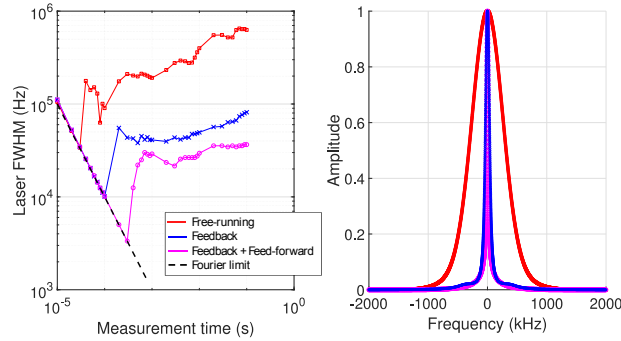


Fig. 10. Reconstruction of the laser spectrum in monochromatic operation using the calibrated output signal of a commercial optical frequency discriminator. (a) Laser linewidth (estimated as the FWHM of the reconstructed laser lineshape) for various integration times between $10 \mu\text{s}$ and 100 ms. The dashed black line represents the Fourier uncertainty that limits the linewidth derivation [32]. (b) Reconstructed laser lineshape for free-running laser (red), feedback-locked laser (blue) and feedback + feed-forward locked laser (magenta), where the frequency noise is integrated over 100 ms.

4. Implementation of the four-stage correction on complex laser chirps

In this section we test our complete, multistage correction (including pre-distorsion, iterative correction, feedback and feed-forward) on complex frequency excursions on our DBR laser. Two configurations are studied, namely triangular excursions, and the arbitrary excursion with 750 MHz by $2.5 \mu\text{s}$ chirps described in Section 2.3.

It is important to realize that the feedback and feed-forward correction can only correct relatively small frequency errors. The initial pre-distorsion and iterative corrections, limiting the error to within a few MHz, are an absolute pre-requisite to ensure the proper action of the real-time correction stages. In their absence, the laser frequency error may largely exceed the MZI free spectral range, making the error signal unreliable.

4.1. Triangular excursions

The feedback and feed-forward corrections are implemented on triangular frequency excursions, using the pre-distorted and iteratively corrected voltage command obtained as described in Section 2. The laser instantaneous frequency is measured using the backwards MZI (see Figure 9) and compared to the desired frequency excursion. The instantaneous frequency error and the optical beatnote spectrum are shown in Figure 11. The corresponding RMS frequency

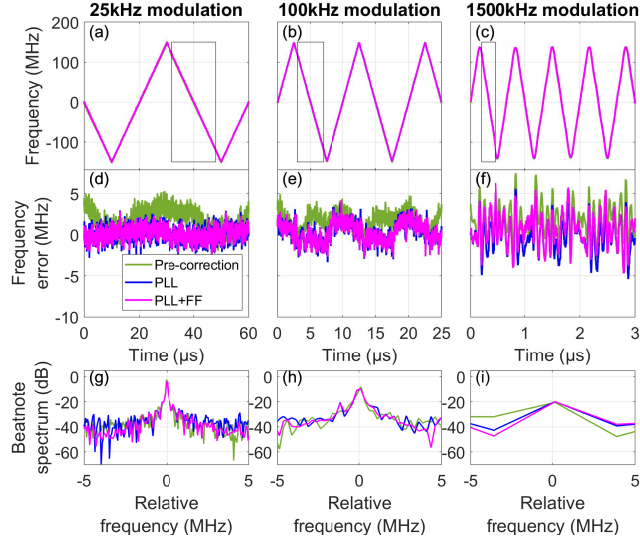


Fig. 11. Implementation of the feedback and feed-forward correction stages on 300 MHz peak-peak triangular excursions with 25, 100 and 1500 kHz modulation frequencies. The green lines correspond to the free-running laser behaviour, after pre-distortion and iterative correction of the command voltage. The blue and magenta lines correspond to the laser behaviour with the combination of pre-distortion and iterative correction with feedback correction (blue), and with feedback and feed-forward correction (magenta). For every configuration we plot the frequency excursions (a, b, c), the frequency errors (d, e, f), and the beatnote spectra (g, h, i). The latter are computed on the rectangles shown in (a) (b) and (c), corresponding to 90% of the downwards linear chirp. For fast modulation rates (i), the beatnote spectrum is computed over a sub- μ s timescale, making the resolution bandwidth very low.

error, computed on several periods including the abrupt slope changes, is given in Table 1.

$f_{\text{modulation}}$	$\sigma_{\text{iteration}}$	σ_{PLL}	$\sigma_{\text{PLL+FF}}$	relative RMS
25 kHz	2.17 MHz	0.79 MHz	0.68 MHz	0.23%
100 kHz	1.99 MHz	1.24 MHz	1.19 MHz	0.40%
1500 kHz	2.77 MHz	2.19 MHz	2.06 MHz	0.69%

Table 1. Frequency fluctuation performances for triangular excursions with 300 MHz span. Note that the value of the RMS is computed over several periods of the triangular wave, including the abrupt slope changes.

The feedback correction visibly enhances the overall chirp precision for all the configurations shown, notably in terms of RMS frequency error. Nevertheless, the feedback bandwidth limits the correction efficiency as one reaches for higher modulation frequencies.

The feed-forward correction further improves the frequency excursion by correcting fluctuations at a faster rate. This is particularly visible in the beatnote spectra where the feed-forward significantly reduces the noise a few MHz away from the center frequency. Nevertheless the sharp angles of the triangular command lead to residual high frequency fluctuations, even with the feed-forward part (see Table 1). We attribute this limitation to the detection noise that is

imparted onto the laser emission via the feedback and feed-forward (see Appendix A). The relative RMS remains well below 1% for all the configurations shown. Note that due to its low-frequency cutoff, the feed-forward correction cannot operate without the feedback correction, due to significant slow frequency noise.

In Table 2 we provide a brief review of recent publications addressing steep laser linear chirps. We compare them with the full four-stage correction presented in Fig. 11, using the RMS frequency error computed only in the linear sections of the triangular excursions, *ie* avoiding the slope changes. The MHz-range precision that we reach, even with extreme chirp rates, demonstrates the versatility of our approach.

Reference	Frequency span	Sweep duration	Chirp rate	RMS frequency error in linear section
[21]	50 GHz	100 ms	0.5 THz/s	0.09 MHz
[22]	4.8 THz	0.8 s	6 THz/s	0.2 MHz
This work	300 MHz	20 μ s	15 THz/s	0.74 MHz
[18]	1.8 GHz	50 μ s	36 THz/s	0.9 MHz
[20]	26 GHz	0.5 ms	52 THz/s	1.5 MHz
This work	300 MHz	5 μ s	60 THz/s	0.83 MHz
[17]	20 GHz	250 μ s	80 THz/s	< 1 MHz
[2]	36 GHz	100 μ s	360 THz/s	1 MHz
[23]	25 GHz	50 μ s	500 THz/s	1.04 MHz
This work	300 MHz	0.33 μ s	910 THz/s	1.63 MHz

Table 2. Comparison of chirp linearities with recently published works, ordered by increasing chirp rates.

We also test our full multi-stage correction on triangular shapes with increasing chirp span Δf , keeping the modulation frequency at 25 kHz and 100 kHz. The results are presented in Table 3. Consistently with our earlier findings, we find that each correction stage successfully improves the frequency excursion accuracy. Interestingly, we show that the relative RMS improves with increasing chirp span, reaching approximately 0.1% with GHz chirp spans.

f_{mod}	Δf	$\sigma_{iteration}$	σ_{PLL}	σ_{PLL+FF}	relative RMS
100kHz	300MHz	1.99MHz	1.24MHz	1.19 MHz	0.40%
	550MHz	1.94MHz	1.43MHz	1.14MHz	0.21%
	800MHz	2.26MHz	1.55MHz	1.46MHz	0.18%
25kHz	300MHz	2.17MHz	0.79MHz	0.68MHz	0.23%
	750 MHz	2.48MHz	1.19MHz	1.04MHz	0.14%
	1200 MHz	2.26MHz	1.55MHz	1.46MHz	0.12%

Table 3. Frequency fluctuation RMS frequency error and relative RMS for triangular excursions with various modulation frequencies and chirps spans.

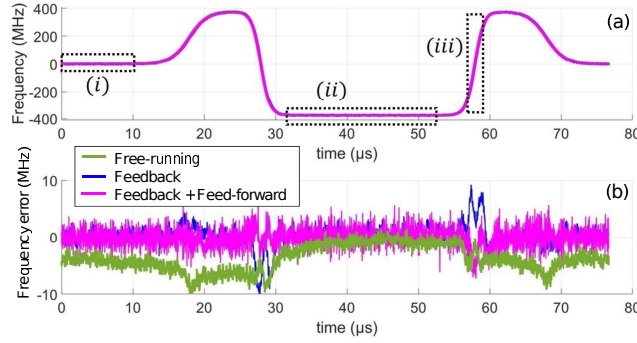


Fig. 12. Laser response (a) and respective frequency errors (b) for an arbitrary frequency excursion. The green line corresponds to the free-running laser behaviour using the pre-distorted and iteratively corrected voltage command. The blue and magenta lines correspond to the same voltage command combined with feedback correction, and combined with feedback correction and FF correction, respectively. The RMS frequency error is retrieved in the three rectangular frames: $\sigma_{FF} = 1.45$ MHz and 1.62 MHz and 1.42 MHz for (i), (ii) and (iii), respectively.

4.2. Arbitrary excursions

We now study the effect of our multi-stage correction on the arbitrary frequency excursion, using the pre-distorted and iteratively corrected voltage command described in Section 2 (see Fig. 12).

Similarly to the triangular excursions, the feedback loop only corrects the low frequency fluctuations and adds high-frequency noise. The feed-forward correction efficiently complements the feedback loop as it strongly reduces the remaining frequency excursion imprecisions that occurred at the steep frequency variation points. Remarkably, the RMS frequency error evaluated on the intermediate monochromatic stage (ii) is only marginally deteriorated with respect to the initial RMS error before the 800 MHz-range perturbation (i). We compute the laser lineshape in the $22 \mu\text{s}$ interval between the two chirps (ii) and obtain a 48 kHz linewidth, close to the Fourier-transform limit, demonstrating the excellent laser spectral purity although in the midst of an abrupt frequency excursion. Finally, the RMS error in the linear part of the positive slope (500 MHz/ $2 \mu\text{s}$) at the end of the arbitrary sequence (iii) is as low as that in monochromatic operation (i). This highlights our multi-stage correction's versatility, *ie* its ability to operate on a succession of abrupt frequency chirps and monochromatic operation.

5. Conclusion

A current-modulated laser can be used to generate fast arbitrary frequency excursions with high modulation frequency and large chirp span. However, the inaccuracy of the frequency excursion and the high-frequency fluctuations induced by the fast spectral components of the modulation calls for an efficient and broadband correction design. In this work, a multi-stage correction is developed, including pre-distortion and iterative correction to suppress systematic errors, and the combination of a feedback loop and a feed-forward correction both based on a self-heterodyne, unbalanced interferometer to suppress both slow and fast stochastic errors up to 5 MHz.

We test our multi-stage correction on various laser frequency excursions to demonstrate its efficiency and versatility. In monochromatic operation we demonstrate an impressive reduction of the laser linewidth with the combined feedback and feed-forward stages. We also achieve 300-MHz triangular excursions with a relative RMS below 1% with modulation frequencies up to 1500 kHz. Finally, we implement this multi-stage correction on an arbitrary frequency excursion

with alternating steep slopes and monochromatic segments, and consistently demonstrate < 100kHz laser spectral purity even in the midst of GHz-scale excursions.

This work opens new possibilities in various application domains including FMCW lidar, telecommunications or wideband signal processing, where fast and accurate laser frequency excursions are required.

A. Appendix: Parameters of the feedback loop

In this section we discuss the relation between the feedback loop parameters and its bandwidth. First, PLL general considerations are presented and applied to our MZI-based feedback loop. Then the influence of the PLL delay on the feedback bandwidth and error correction is studied. Finally, the MZI delay impact on the laser instantaneous frequency measurement and the buildup of the error signal is discussed.

A.1. PLL transfer function

A PLL generally contains the following elements: a local oscillator, a phase comparator, a loop filter, and a voltage-controlled oscillator (VCO) [34]. The Open Loop Transfer Function (OLTF) is the product of the transfer functions of the successive elements of the loop:

$$F_{OL}(f) = \frac{1}{2i\pi f} K_{\Phi} F_{lf}(f) K_{VCO}(f), \quad (5)$$

where K_{Φ} is the phase comparator gain such that, when two signals with a $\Delta\Phi$ phase difference are sent to the phase comparator, the following signal is output: $V = K_{\Phi}\Delta\Phi$. $F_{lf}(f)$ is the loop filter transfer function, and $K_{VCO}(f)$ is the VCO transfer function. Finally, the Closed Loop Transfer Function (CLTF) is given by:

$$F_{CL}(f) = \frac{F_{OL}(f)}{1 + F_{OL}(f)} \quad (6)$$

In the case of feedback correction on a current-controlled laser (see Section 3 and Figure 6), the VCO includes the laser driver, the laser source and the MZI. Its transfer function, given by $H(f)$, is described and measured in section 2.3 (see Fig. 3). The loop filter is comprised of the servo-controller in PI mode, and a passive, 5-th order low-pass filter with a 10 MHz cutoff frequency, whose transfer functions are measured separately. The phase comparator, whose role is ensured by the mixer, is also characterized and found to give rise to a significant group delay together with a constant dephasing, so we write $F_{\Phi}(f) = K_{\Phi} e^{-2i\pi f \tau_{mix} - i\Phi_{mix}}$, with $\tau_{mix} = 50$ ns and $\Phi_{mix} = \pi/4$. Finally the various delays induced by each element of the feedback loop are summarized in Table 4. Finally the OLTF reads as:

$$F_{OL}(f) = \frac{1}{2i\pi f} F_{\Phi}(f) F_{PI}(f) F_{lp}(f) H(f) \quad (7)$$

We measure the feedback loop transfer function $F_{CL}(f)$ by making the laser frequency oscillate with the feedback loop closed. A small amplitude (8 MHz), monochromatic frequency modulation is applied on the local oscillator. The closed PLL ensures that the phase of the MZI output matches the phase of the local oscillator, which induces a frequency modulation of the laser source. The resulting instantaneous frequency variations of the laser emission are measured by analyzing the beatnote at the output of the MZI, giving access to the PLL transfer function plotted in Fig. 7. The dynamic range of the gain measurement is limited because the feedback loop parameters must be kept constant for all frequencies, rendering impossible to compensate for the strong attenuation of frequencies above 500 kHz. In order to accurately account for the experimental transfer function measurements, the simulated transfer function

Component	Transfer function	Group delay
Laser+MZI	$H(f)$	100 ns
LB1005	$F_{PI}(f)$	40 ns
Mixer	$F_{\Phi}(f)$	50 ns
Low-pass filter	$F_{lp}(f)$	44 ns

Table 4. Effective group delays induced by each element of the feedback loop.

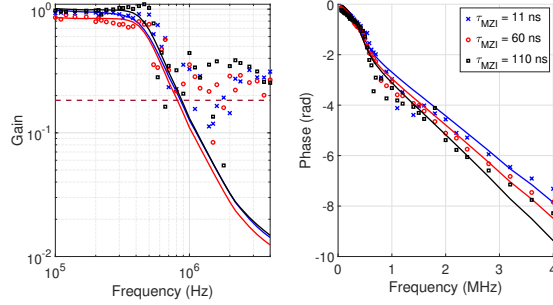


Fig. 13. PLL transfer function for 3 different MZI delays: 11 ns, 60 ns and 110 ns. PLL transfer function measurements are plotted for 3 different MZI delays: 11 ns (blue points), 60 ns (red points) and 110 ns (black points). The corresponding theoretical transfer functions for each MZI delay are computed using equations 5 and 6 with the transfer functions of the PLL elements and the corresponding MZI delay: 11 ns (blue line), 60 ns (red line) and 110 ns (black line)

given by Eqs. 6 and 7 is corrected by a small additional delay ($\tau_{\text{extra}} = 101$ ns), ascribed to the various electronic and optical delays present in the loop and not explicitly considered in our analysis (free space propagation, coaxial cables, splitters, etc). The simulation finally provides a good understanding of the PLL transfer function, and allows us to estimate the total group delay associated to the feedback loop $\tau_{\text{PLL}} = 335$ ns, accounting for all its components.

We now explore the impact of the MZI delay on the PLL transfer function. To that end we operate the laser with the feedback correction using various fiber lengths in the MZI (such that $\tau_{\text{MZI}} = 11$ ns, 60 ns and 110 ns). The results plotted in Figure 13 show only a weak dependence of the PLL transfer function, confirming that the MZI delay only contributes marginally to the feedback bandwidth.

A.2. PLL delay and feedback bandwidth

In this section we examine how the group delay-like behavior of the PLL transfer function leads to a bandwidth limitation. Let us assume that the laser exhibits a sinusoidal frequency fluctuation $\epsilon_0(t)$ at frequency F with an amplitude ΔF : $\epsilon_0(t) = \Delta F \sin(2\pi Ft)$. If the feedback loop is equivalent to a mere delay line, the feedback signal reads as $U_{fb}(t) = G\epsilon_0(t - \tau_{\text{PLL}})$, where G is the feedback loop gain. After applying the feedback signal to the laser source, the frequency fluctuation becomes $\epsilon(t) = \epsilon_0(t) - U_{fb}(t)$. To quantify the effect of this feedback on the laser frequency stability, we examine the variance $\sigma^2 = \langle \epsilon(t)^2 \rangle$ of the frequency fluctuations:

$$\sigma^2 = \Delta F^2 \left(\frac{G^2 + 1}{2} - G \cos(2\pi F \tau_{\text{PLL}}) \right) \quad (8)$$

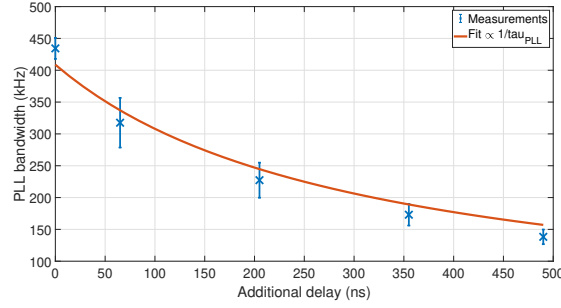


Fig. 14. Exploring the effect of adding coaxial delay lines to the feedback loop on the PLL bandwidth. The laser is operated at fixed frequency and the PLL bandwidth is retrieved from the beatnote spectra (analog to Fig. 8). The experimental points are fitted using Eq. 10 and a value $\tau_{\text{PLL}} = 306 \pm 12$ ns is found.

σ^2 reaches a minimum when $G = \cos(2\pi F \tau_{\text{PLL}})$:

$$\sigma_{\min}^2 = \frac{\Delta F^2}{2} \sin^2(2\pi F \tau_{\text{PLL}}) \quad (9)$$

The fluctuation variance with no feedback is $\sigma_0^2 = \frac{\Delta F^2}{2}$. The ratio $\frac{\sigma_{\min}^2}{\sigma_0^2}$ can be seen as the feedback loop's ability to correct fluctuations at frequency F . To lowest order, this figure of merit quadratically increases with the fluctuation frequency F . We define the feedback loop bandwidth as the frequency F for which the aforementioned variance ratio is equal to $\frac{1}{2}$:

$$F_{\text{BW}} = \frac{1}{8\tau_{\text{PLL}}} \quad (10)$$

This confirms the common knowledge that a large feedback bandwidth requires a short loop delay τ_{PLL} .

We experimentally examine the influence of the total loop delay on the feedback loop performance. The laser is operated at fixed frequency and the feedback bandwidth is retrieved from the beatnote spectra (analog to Fig. 8). Several values of the PLL delay are explored by adding coaxial delay lines to the existing setup, leading to a total PLL length $\tau_{\text{PLL}} + \tau_{\text{coax}}$. The measured bandwidths are shown in Figure 14 and show a $1/(\tau_{\text{PLL}} + \tau_{\text{coax}})$ scaling law, in agreement with Eq. 10. By fitting the measurements with the model, we derive $\tau_{\text{PLL}} = 306 \pm 12$ ns.

A.3. MZI delay influence on instantaneous frequency measurement

Although the MZI delay only marginally affects the PLL transfer function and bandwidth, it actually influences the laser frequency measurement precision, because it is involved in the derivation of the error signal. In the following we show that the ideal MZI delay results from a compromise between precision and sensitivity to detection noise.

Instantaneous frequency accuracy We first analyze how the MZI delay comes into play in the laser instantaneous frequency derivation. This derivation starts with the analytical representation of the beatnote signal at the output of the MZI, whose complex phase is $2\pi f_{\text{MZI}}t + \phi(t - \tau_{\text{MZI}}) - \phi(t)$. After removing the linear term due to the frequency shift $2\pi f_{\text{MZI}}t$, one is left with the laser phase variation $\phi(t - \tau_{\text{MZI}}) - \phi(t)$, from which the laser instantaneous frequency is derived:

$$f(t) = -\frac{1}{2\pi} \frac{d\Phi}{dt} \approx -\frac{1}{2\pi} \frac{\Phi(t) - \Phi(t - \tau_{\text{MZI}})}{\tau_{\text{MZI}}} \quad (11)$$

This estimation of the instantaneous frequency is not perfectly accurate. For example, in the case of a linear frequency chirp $\phi(t) = \pi r t^2$, Eq. 11 leads to a $\frac{1}{2} r \tau_{\text{MZI}}$ inaccuracy of the instantaneous frequency estimation. This inaccuracy increases with the MZI delay [28].

Sensitivity to detection noise On the other hand, shorter delays increase the sensitivity to detection noise. When the laser is perfectly stable with no frequency drift ($f(t) = 0$), the beatnote signal captured by the photodiode is a sinusoid oscillating at the AOM frequency: $V(t) = V_0(1 + \sin(2\pi f_{\text{MZI}}t))$. In the presence of a monochromatic detection noise at frequency F , the voltage becomes $V(t) = V_0(1 + \sin(2\pi f_{\text{MZI}}t)) + A \sin(2\pi F t)$. Once the constant term V_0 is removed, its instantaneous phase $\psi(t)$ is obtained as the complex argument of the analytic representation of $V(t)$ [28]. Assuming $A \ll V_0$, one obtains:

$$\psi(t) = 2\pi f_{\text{MZI}}t + \frac{A}{V_0} \sin(2\pi(F - f_{\text{MZI}})t) \quad (12)$$

After removing the linear phase coming from the fixed frequency shift in the MZI ($2\pi f_{\text{MZI}}t$), the remaining term is multiplied by $\frac{1}{2\pi\tau_{\text{MZI}}}$ to derive the instantaneous frequency (according to Equation 11):

$$f(t) = \frac{\frac{A}{V_0}}{2\pi\tau_{\text{MZI}}} \sin(2\pi(F - f_{\text{MZI}})t) \quad (13)$$

Therefore the instantaneous frequency derivation converts the detection noise into instantaneous frequency measurement noise. The variance of such frequency fluctuations is given by:

$$\sigma_{\text{det}}^2(F) = \frac{\left(\frac{A}{V_0}\right)^2}{8\pi^2\tau_{\text{MZI}}^2} \quad (14)$$

This frequency-independent, $1/\tau_{\text{MZI}}^2$ scaling law shows that a long MZI delay minimizes the influence of electronic noise.

Generalizing to a white detection noise, the power spectral density of the apparent laser frequency noise should also scale as $1/\tau_{\text{MZI}}^2$. We verify this by measuring the free-running laser frequency variance using different MZI delay lengths (see Fig. 15). We observe that the frequency noise variance is compatible with the sum of two terms:

$$\sigma^2 = \sigma_{\text{laser}}^2 + \sigma_{\text{det}}^2 \quad (15)$$

where σ_{laser}^2 is the native laser frequency noise variance and $\sigma_{\text{det}}^2 \propto 1/\tau_{\text{MZI}}^2$ corresponds to the contribution of detection noise.

Conclusion As a result, although the MZI delay has little influence on the PLL bandwidth, it has a strong impact on the accuracy of the instantaneous derivation on the one hand, and on the transduction of electronic noise onto the instantaneous frequency measurement. We finally choose a delay of 60 ns, as a compromise between precision and sensitivity to detection noise.

B. Appendix: Feed-forward

In this section we discuss the feed-forward theoretical transfer function and the influence of the EOM delay. We show that the optimal delay can be determined by minimizing the laser linewidth.

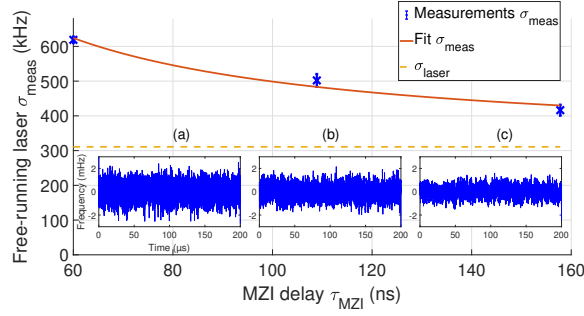


Fig. 15. Influence of the MZI delay on the occurrence of detection noise. The RMS frequency error is measured over a 200 μs interval for different MZI delays. The laser is operated in free-running mode (no feedback or feed-forward) at fixed frequency. The measurements are fitted using Eq. 15 with $\sigma_{\text{laser}} = 310$ kHz. Insets: corresponding instantaneous frequency measurements: (a) $\tau_{\text{MZI}} = 60$ ns (b) 108.9 ns and (c) 158 ns.

Component	Transfer function	Group delay
EOM	$F_{\text{MZI}}(f)F_{\text{EOM}}(f)$	90 ns
Mixer	$F_{\Phi}(f)$	50 ns
LB1005	$F_{\text{PI}}(f)$	40 ns
Low-pass filter	$F_{\text{lp}}(f)$	15 ns

Table 5. Effective group delays induced by each element of the feed-forward correction.

B.1. Feed-forward delay

The buildup of the feed-forward correction signal is subject to a time delay τ_{FF} owing to the various optical and electronic components of the feed-forward setup:

$$\tau_{\text{FF}} = \frac{-1}{2\pi} \frac{\partial \Phi_{\text{FF}}}{\partial f} \quad (16)$$

where

$$\Phi_{\text{FF}} = \arg [F_{\text{MZI}}(f)F_{\Phi}(f)F_{\text{FF}}(f)F_{\text{lp}}(f)F_{\text{EOM}}(f)] \quad (17)$$

F_{MZI} , F_{Φ} , F_{FF} , F_{lp} , F_{EOM} are the transfer functions of the MZI, the phase comparator, the feed-forward PI filter, the low-pass filter, and the electro-optic modulator, respectively. Some of these transfer functions can be measured independently, namely F_{Φ} , F_{FF} , and F_{lp} . Measuring the transfer function of an EOM requires a means to measure an instantaneous frequency in the optical domain. This is why it is most convenient to measure the combined transfer functions of the EOM and the MZI: $F_{\text{MZI}}(f)F_{\text{EOM}}(f)$. We are finally able to compute the product of all these transfer functions, and we plot them in Fig. 16. We find that the feed-forward signal is high-pass filtered due to the derivator behaviour of the EOM. It exhibits a linear phase $\Phi_{\text{FF}}(f)$, indicating an effective group delay $\tau_{\text{FF}} = 183$ ns. This delay corresponds to the sum of all individual group delays of each element of the feed-forward correction, which are specified in Table 5.

B.2. Influence of EOM delay mismatch

The feed-forward optimally corrects the laser frequency deviations when the delay τ_{FF} experienced by the correction signal to reach the EOM matches the physical delay τ_{EOM} experienced

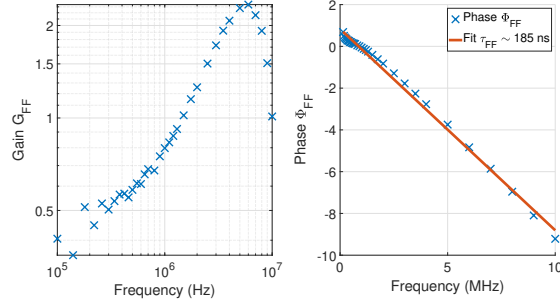


Fig. 16. Feed-forward transfer function. The feed-forward exhibits a high-pass behaviour due to the derivator behavior of the EOM. Nevertheless, a cutoff is observed above 5 MHz due to the MZI response, determining the FF bandwidth. The ideal length of the fibered delay line τ_{EOM} is derived from the slope of the transfer function phase (see Eq. 17).

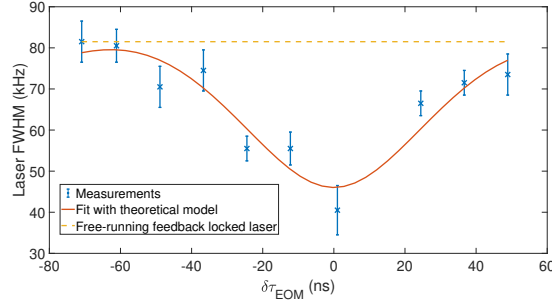


Fig. 17. Influence of a feed-forward delay mismatch $\delta\tau_{\text{EOM}}$ on the laser linewidth (10 ms integration time). The latter is measured with a stabilized optical frequency discriminator (SilentSys). Zero $\delta\tau_{\text{EOM}}$ corresponds to the optimised FF delay.

by the laser beam to reach that same device. In this section we study the influence of a feed-forward delay mismatch $\delta\tau_{\text{EOM}}$ on the laser linewidth. To that end we unfold a simple theoretical approach.

Let us first assume that the laser source exhibits a sinusoidal frequency fluctuation $\epsilon_0(t) = \Delta F \sin(2\pi Ft)$. We consider that the feed-forward correction signal $G\epsilon_0(t - \delta\tau_{\text{EOM}})$ is applied to the EOM with a temporal mismatch $\delta\tau_{\text{EOM}}$, leading to a corrected frequency fluctuation:

$$\epsilon(t) = \Delta F (\sin [2\pi Ft] - G \sin [2\pi F(t - \delta\tau_{\text{EOM}})]) \quad (18)$$

The frequency fluctuation variance $\sigma^2(F)$, defined as: $\sigma^2 = \langle \epsilon(t)^2 \rangle$ is given by:

$$\sigma^2(F) = \Delta F^2 \left(\frac{G^2 + 1}{2} - G \cos(2\pi F \delta\tau_{\text{EOM}}) \right) \quad (19)$$

We now consider that the laser is affected by a white frequency noise, *ie* the perturbation is uniform for all frequencies. The laser linewidth is proportional to the total variance of the laser frequency fluctuations [35]:

$$\sigma_{\text{tot}}^2 = \frac{1}{F_{\text{max}} - F_{\text{min}}} \int_{F_{\text{min}}}^{F_{\text{max}}} \sigma^2(F) dF \quad (20)$$

where F_{max} and F_{min} are the maximum and minimum frequency addressed by the feed-forward correction. Assuming $F_{min} \ll F_{max}$, one obtains:

$$\sigma_{tot}^2 = \Delta F^2 \left(\frac{G^2 + 1}{2} - G \frac{\sin(2\pi\delta\tau_{EOM}F_{max})}{2\pi\delta\tau_{EOM}F_{max}} \right) \quad (21)$$

This expression shows that the laser linewidth is minimal when $\delta\tau_{EOM} = 0$, in agreement with empirical measurements reported in [25]. It also highlights that finding such a minimum is easier when the feed-forward bandwidth is reduced. We verify this behaviour by measuring the DBR laser linewidth with a range of values for the EOM delay around the optimal τ_{EOM} , using optical fibers with different lengths (see Figure 17). Fitting the experimental data with expression 21, we find the actual feed-forward correction bandwidth $F_{max} = 5.7 \pm 0.6$ MHz.

Funding. The authors acknowledge support from the French National Research Agency (ANR) through the ATRAP project (ANR-19-CE24-0008). This work has received support under the program “Investissements d’Avenir” launched by the French Government.

Acknowledgments. The authors are grateful to Michel Lintz and Vincent Crozatier for helpful discussions.

Disclosures. The authors declare no conflicts of interest.

Data availability. Data underlying the results presented in this paper are not publicly available at this time but may be obtained from the authors upon reasonable request.

References

1. I. Gazizov, S. Zenevich, and A. Rodin, “Low-pixel-count imaging fmcw lidar,” *Appl. Opt.* **61**, 9241–9246 (2022).
2. X. Zhang, J. Pouls, and M. C. Wu, “Laser frequency sweep linearization by iterative learning pre-distortion for fmcw lidar,” *Opt. Express* **27**, 9965–9974 (2019).
3. L. A. Kranendonk, R. J. Bartula, and S. T. Sanders, “Modeless operation of a wavelength-agile laser by high-speed cavity length changes,” *Opt. Express* **13**, 1498–1507 (2005).
4. W. R. Babbitt, Z. W. Barber, S. H. Bekker, *et al.*, “From spectral holeburning memory to spatial-spectral microwave signal processing,” *Laser Phys.* **24**, 094002 (2014).
5. A. Kinoshita, D. Hunger, R. Kolesov, *et al.*, “Roadmap for rare-earth quantum computing,” arXiv preprint arXiv:2103.15743 (2021).
6. L. Levin, “Mode-hop-free electro-optically tuned diode laser,” *Opt. letters* **27**, 237–239 (2002).
7. V. Crozatier, G. Gorju, F. Bretenaker, *et al.*, “Phase locking of a frequency agile laser,” *Appl. Phys. Lett.* **89** (2006).
8. M. Li, L. Chang, L. Wu, *et al.*, “Integrated Pockels laser,” *Nat. communications* **13**, 5344 (2022).
9. R. Nagarajan and J. E. Bowers, “High-speed lasers,” *Semicond. Lasers I* pp. 177–290 (1999).
10. L. Westbrook, A. Nelson, P. Fiddymant, and J. Collins, “Monolithic 1.5 μm hybrid DFB/DBR lasers with 5 nm tuning range,” *Electron. letters* **23**, 957–959 (1984).
11. X. Pan, H. Olesen, and B. Tromborg, “Modulation characteristics of tunable DFB/DBR lasers with one or two passive tuning sections,” *IEEE J. Quantum Electron.* **25**, 1254–1260 (1989).
12. W. Zheng and G. Taylor, “Determination of the photon lifetime for dfb lasers,” *IEEE J. Quantum Electron.* **43**, 295–302 (2007).
13. W. Yi, Z. Li, Z. Zhou, *et al.*, “Frequency-modulated chirp signals for single-photodiode based coherent lidar system,” *J. Light. Technol.* **39**, 4661–4670 (2021).
14. M. Laroche, C. Bartolacci, G. Lesueur, *et al.*, “Serrrodyne optical frequency shifting for heterodyne self-mixing in a distributed-feedback fiber laser,” *Opt. letters* **33**, 2746–2748 (2008).
15. I. Y. Poberezhskiy, B. Bortnik, J. Chou, *et al.*, “Serrrodyne frequency translation of continuous optical signals using ultrawide-band electrical sawtooth waveforms,” *IEEE journal quantum electronics* **41**, 1533–1539 (2005).
16. N. Satyan, A. Vasilyev, G. Rakuljic, *et al.*, “Precise control of broadband frequency chirps using optoelectronic feedback,” *Opt. express* **17**, 15991–15999 (2009).
17. G. Kervella, J. Maxin, M. Faugeron, *et al.*, “Laser sources for microwave to millimeter-wave applications,” *Photonics Res.* **2**, B70–B79 (2014).
18. G. Lihachev, A. Bancora, V. Snigirev, *et al.*, “Frequency agile photonic integrated external cavity laser,” arXiv preprint arXiv:2303.00425 (2023).
19. P. Li, T. Yang, J. Yang, *et al.*, “The nonlinear tuning technique of a DFB laser using frequency predistortion procedures,” in *Terahertz, RF, Millimeter, and Submillimeter-Wave Technology and Applications XIII*, vol. 11279 (SPIE, 2020), pp. 250–255.

20. X. Cao, K. Wu, C. Li, *et al.*, "Highly efficient iteration algorithm for a linear frequency-sweep distributed feedback laser in frequency-modulated continuous wave lidar applications," *JOSA B* **38**, D8–D14 (2021).
21. J. Qin, Q. Zhou, W. Xie, *et al.*, "Coherence enhancement of a chirped dfb laser for frequency-modulated continuous-wave reflectometry using a composite feedback loop," *Opt. letters* **40**, 4500–4503 (2015).
22. P. A. Roos, R. R. Reibel, T. Berg, *et al.*, "Ultrabroadband optical chirp linearization for precision metrology applications," *Opt. letters* **34**, 3692–3694 (2009).
23. P. Li, Y. Zhang, and J. Yao, "Linear frequency swept laser source with high swept slope based on digital optical phase-locked loop," *Opt. Commun.* **525**, 128860 (2022).
24. C. Greiner, B. Boggs, T. Wang, and T. Mossberg, "Laser frequency stabilization by means of optical self-heterodyne beat-frequency control," *Opt. letters* **23**, 1280–1282 (1998).
25. M. Lintz, D.-H. Phung, J.-P. Coulon, *et al.*, "Note: Efficient diode laser line narrowing using dual, feed-forward+feed-back laser frequency control," *Rev. Sci. Instruments* **88** (2017).
26. Y. S. Cheng, B. Szutor, and D. T. Reid, "Feed-forward stabilization of a single-frequency, diode-pumped Pr:YLF-Cr:LiCAF laser operating at 813.42 nm," *Opt. Express* **30**, 42902–42911 (2022).
27. J. Zhang, C. Gao, M. Xue, and R. Liu, "Research on frequency modulation character of the current driven dfb semiconductor laser," *Mod. Phys. Lett. B* **33**, 1850422 (2019).
28. T.-J. Ahn and D. Y. Kim, "Analysis of nonlinear frequency sweep in high-speed tunable laser sources using a self-homodyne measurement and hilbert transformation," *Appl. optics* **46**, 2394–2400 (2007).
29. M. Funabashi, H. Nasu, T. Mukaiharu, *et al.*, "Recent advances in DFB lasers for ultradense WDM applications," *IEEE J. selected topics quantum electronics* **10**, 312–320 (2004).
30. F. Aflatouni and H. Hashemi, "Wideband tunable laser phase noise reduction using single sideband modulation in an electro-optical feed-forward scheme," *Opt. Lett.* **37**, 196–198 (2012).
31. G. Di Domenico, S. Schilt, and P. Thomann, "Simple approach to the relation between laser frequency noise and laser line shape," *Appl. optics* **49**, 4801–4807 (2010).
32. N. Von Bandel, M. Myara, M. Sellahi, *et al.*, "Time-dependent laser linewidth: beat-note digital acquisition and numerical analysis," *Opt. Express* **24**, 27961–27978 (2016).
33. G. M. Stéphan, T. Tam, S. Blin, *et al.*, "Laser line shape and spectral density of frequency noise," *Phys. Rev. A* **71**, 043809 (2005).
34. A. Blanchard, *Phase-locked loops: Application to coherent receiver design* (1976).
35. D. S. Elliott, R. Roy, and S. J. Smith, "Extracavity laser band-shape and bandwidth modification," *Phys. Rev. A* **26**, 12–18 (1982).